

Coulomb blockade in two island systems with highly conductive junctions

Bernhard Limbach, Peter vom Stein, Christoph Wallisser, and Roland Schäfer

Forschungszentrum Karlsruhe, Institut für Festkörperphysik

Postfach 3640, 76021 Karlsruhe, Germany

(Dated: November 25, 2017)

We report measurements on single-electron pumps, consisting of two metallic islands formed by three tunnel junctions in series. We focus on the linear-response conductance as a function of gate voltage and temperature of three samples with varying system parameters. In all cases, strong quantum fluctuation phenomena are observed by a $\log(k_B T / (2E_{co}))$ reduction of the maximal conductance, where E_{co} measures the coupling strength between the islands. The samples display a rich phenomenology, culminating in a non-monotonic behavior of the maximal conductance as a function of temperature.

PACS numbers: 73.23.Hk, 85.35.Gv, 73.40.Gk

The transport properties of single electron devices are well described by the so called sequential tunneling model as long as the conductances of the underlying tunneling contacts are small compared to the conductance quantum $G_K = e^2/h$ [1, 2]. In most practical cases, however, one has to include higher-order corrections for a quantitative description due to quantum fluctuations of the charge number on the single electron islands. This has been demonstrated clearly for the single electron transistor (SET) [3, 4, 5, 6, 7]. Excellent agreement between experimental investigations and theoretical studies has been established at low conductances with the aid of perturbation expansion including the correct description of a logarithmic contribution to the linear-response conductance of the multichannel-Kondo type. At higher conductances however, perturbation theory breaks down. Nevertheless, by applying Monte-Carlo methods, the experimental results can be described with amazingly high accuracy [3, 5, 8]. The findings on the SET indicate that a close match between the model Hamiltonian and its experimental realization exists for single electron devices. It is not clear a priori whether the good agreement between perturbation expansion and experiment as well as Quantum-Monte-Carlo numerics found for the SET survives if more complex arrangements of single electron islands are investigated. E. g. the low temperature conductance of the SET involves finite occupation of only two states and the mapping onto the multichannel-Kondo model is based on identifying those two states with a pseudo spin. This procedure has no simple analogy in general arrangements. It is worthwhile to check the range of validity of perturbation theory in more general cases. Two island systems, readily accessible both by experiment and theory, serve as a good starting point.

In this Letter we present an experimental study of the linear-response conductance of two single electron islands in series, an arrangement nicknamed single electron pump (SEP) [9, 10, 11] and sketched in Fig. 1. The linear-response conductance varies with the gate voltages and is bound between temperature dependent val-

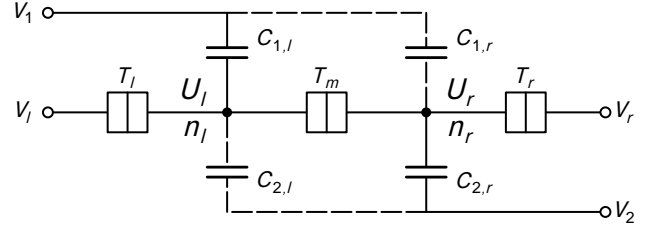


FIG. 1: Schematic representation of the single-electron pump. The three tunneling contacts T_l , T_m , and T_r are laid out in a row forming two islands (each contact $i \in \{l, m, r\}$ is characterized by its capacitance C_i and conductance $G_i \equiv g_i G_K$). n_l and n_r count the number of electrons by which the left and right island charge differs from neutrality. The arrangement is biased by the voltage difference $V_r - V_l$. The electrostatic potentials on the islands (U_l and U_r) can be tuned by V_1 and V_2 which couple directly to the islands by the capacitances C_{1l} and C_{2r} . C_{2l} and C_{1r} represent the experimentally unavoidable stray capacitances.

ues $G_{\min}(T)$ and $G_{\max}(T)$. For samples in an interesting and accessible parameter range, the maximal conductance G_{\max} obeys a non-monotonic behavior as a function of temperature, which is reported here for the first time. This behavior, astonishing at first sight, is naturally explained by the sequential tunneling model in this Letter, giving evidence that non trivial behavior is to be expected in complex arrangements of single-electron islands. Beyond the validity range of the sequential model, we find a logarithmic correction of the conductance at low temperature due to quantum fluctuations. Our high quality data make a sensitive test of perturbation theory as developed e. g. in Ref. 12 feasible. This however, requires an elaborate calculation along the line of formulae in Ref. 12, which is out of the scope of the work presented here.

The linear-response conductance of the SEP can be modeled in various coordinate systems spanning the (V_1, V_2) plane. In this letter we choose dimensionless coordinates n_x and n_y defined such that the charging energy $E_{ch} = E_{cx}(n_x - n_s)^2 + E_m(n_y + \Delta n + \kappa n_s)^2$. Here

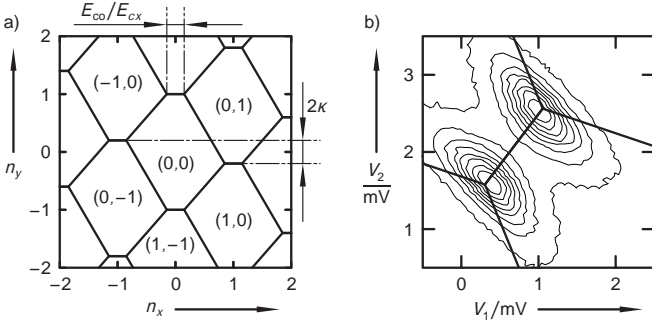


FIG. 2: a) Stability diagram for the SEP sketched in Fig. 1. The hexagonal cells mark regions where the indicated charge state (n_l, n_r) possesses the lowest energy $E_{\text{ch}}(n_l, n_r)$. b) Measurement of the linear-response conductance of sample 2 as a function of both gate voltages V_1 and V_2 at 150 mK. The outermost contour line indicates a conductance of 0.01 μS . The following lines range from 0.05 μS to 0.4 μS with a 0.05 μS spacing. The stability diagram (thick lines) is deformed in the coordinates of this figure.

$E_{cx} = e^2/(2C_s)$ with C_s being the sum of all external capacitances in Fig. 1 (i.e. all capacitances except C_m), $E_m = (e^2/2)C_s/(C_m C_s + C_{sl} C_{sr})$ with C_{sl} and C_{sr} denoting the sum of the external capacitances on the left and the right island separately, and $\kappa = (C_{sr} - C_{sl})/C_s$. The coordinate n_x is associated with the change of the total charge number $n_s = n_l + n_r$, while n_y redistributes the charge between both islands ($\Delta n = n_l - n_r$).

Each point in the plane spanned by n_x and n_y can be mapped onto a charge ground state (n_l, n_r) which gives the lowest possible electrostatic charging energy $E_{\text{ch}}(n_l, n_r)$. This procedure divides the (n_x, n_y) plane into the grid of hexagonal cells depicted in Fig. 2a. The length E_{co}/E_{cx} of the horizontal cell boundaries is a measure of the coupling strength, where $E_{co} = E_{cx} + E_m(\kappa^2 - 1)/4 \propto C_m$. Due to the periodicity it suffices to study the linear-response conductance in a small exemplary portion of the (n_x, n_y) plane. Within the sequential model, the linear-response conductance of the system vanishes exponentially at low temperatures except close to the triple points in the (n_x, n_y) plane, where the ground-state energy of all three adjacent states is degenerate. The conductance peaks near these points. It is worthwhile to mention a peculiar behavior of the SEP: Exactly at the triple points the low temperature conductance is constant and given by $G_0/3$ where $G_0^{-1} = G_l^{-1} + G_r^{-1} + G_m^{-1}$. Although for $T \ll E_{co}/k_B$ the maximal conductance G_{max} is temperature independent as well, the system assumes G_{max} at a slightly different position in the n_x direction [12]. Taking only three states into account (the occupation probability of all other states is exponentially small for $T < E_{co}/k_B$) we get

$$G(n_x)|_{n_y=-\kappa} = \frac{G_s}{2 + e^{-\beta\Delta E}} \left(\frac{g_s}{g_m} + \frac{e^{\beta\Delta E} - 1}{\beta\Delta E} \right)^{-1}, \quad (1)$$

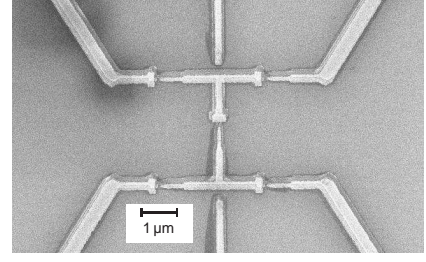


FIG. 3: Scanning electron microscope picture of sample 2. The two T-shaped structures in the middle are the islands. The inner tunneling contact is visible in the center of the picture. The outer contacts are turned by 90° with respect to the former. The gate lines are visible at top and bottom pointing up and down towards the inner contact. In the final measurement the top and bottom leads are biased in parallel.

with $\beta = 1/(k_B T)$, $g_s = g_l g_r / (g_l + g_r) = G_s/G_K$, and $\Delta E = 2E_{cx}(n_x - 1) + E_{co}$. Depending on the ratio g_s/g_m the peak position deviates from the triple point at $\Delta E = 0$ for $g_m \neq 2g_s$.

In a measurement as a function of n_x and n_y the conductance displays a periodic grid of peaks (grouped as pairs), marking the endpoints of the horizontal boundaries in Fig. 2a. With rising temperature the peaks broaden and shift towards the center of the horizontal boundaries. Fig. 2b gives an example at $T = 150 \text{ mK} \sim 0.09 E_{cx}/k_B$, where thermal broadening already is effective in merging the two separate peaks. Finally the two peaks merge completely and the conductance takes its maximal value at the mid-points, e.g. at $n_x = 1$ and $n_y = -\kappa$.

We study three samples in two different layouts. All samples have been produced by standard shadow-evaporation technique from aluminum with aluminum-oxide barriers. The barriers for the middle and outer contacts are fabricated in different oxidation steps, making different barrier thicknesses for internal and external contacts possible. Sample 1 has a simple layout (not shown) with three contacts in a row, which is the most natural arrangement to fabricate a SEP. In this layout the serial conductance is accessible, but the conductance of the individual contacts remains unknown. In the slightly more complex structure of sample 2 and 3 (see Fig. 3) each island is connected to independent leads via two contacts. This permits measuring the conductance of different serial combinations of the contacts, and thus the individual contact conductances can be determined. In the final experiments both external contacts of each island are operated in parallel (connected to the same voltage source), and the two contacts then act exactly as a single contact. We could not detect any degradation (considering noise performance or sensitivity to external disturbances) for the latter samples compared to sample 1.

From the positions of the conductance peaks in the

TABLE I: Parameters of the three samples.

samp.	$\frac{E_{cx}}{k_B}$ (K)	$\frac{E_m}{k_B}$ (K)	$\frac{E_{co}}{k_B}$ (K)	$\frac{E_c}{k_B}$ (K)	κ	g_l	g_r	g_m	G_0 (μ S)
1	2.8	5.8	1.3	5.6	-0.018	0.44	0.44	0.04	1.42
2	1.6	3.0	0.9	2.5	0.10	0.52	0.83	1.32	10.0
3	1.5	4.7	0.3	4.5	0.0013	0.73	0.57	0.03	0.95

(n_x, n_y) plane at low temperatures (see Fig. 2) we obtain the parameters κ and E_{co}/E_{cx} . In addition we measure the conductance in the high temperature region where it does not depend on either n_x nor on n_y . In close analogy to the high temperature expansion for the SET, it behaves as $G(T) \approx G_0 ((1 - E_c/(3k_B T)))$. It can be shown [13, 14] that the relation

$$E_{cx} = \frac{E_c}{G_0} \left(\frac{e_+}{G_l} + \frac{e_-}{G_r} + \frac{e_+ + e_- - 2E_{co}/E_{cx}}{G_m} \right)^{-1}$$

holds, where $e_{\pm} = ((E_{co}/E_{cx})(\kappa \pm 1) \mp 2) / (\kappa \mp 1)$ and E_c is an experimentally determined fitting parameter. Tab. I gives all relevant sample parameters.

To simplify the analysis of our data and facilitate the comparison with theoretical considerations we focus on the temperature dependence of three special values of the conductance in the (n_x, n_y) plane, namely G_{\min} , G_{\max} , and G_m , the latter defined as the conductance at the center of the horizontal boundaries in Fig. 2a (i.e. at $n_x = 1, n_y = -\kappa$). In Fig. 4 we display our main findings. In addition to our experimental results we present the outcome of a calculation in the framework of the sequential tunneling model using the parameters from Tab. I. The techniques for such a calculation are well documented in the literature (e.g. [2]) so we do not comment on this calculation in detail. It requires the solution of a master equation which one may set up using golden rule rates for the inelastic tunneling events. For $T \ll E_c/k_B$ at most four (n_l, n_r) states are occupied with reasonable probability. Restricting the master equation to these four states allows for an analytical solution. At higher temperatures numerical relaxation methods are used.

The sequential tunneling model gives good agreement with our experimental data with the exception of G_{\max} at low temperature. The latter deviations are discussed at the end of the letter. The overall behavior (see Fig. 4) is governed by two scales (E_{co}/k_B and E_c/k_B) at which $G_m(T)$ and $G_{\min}(T)$, respectively, start to increase and finally merge with $G_{\max}(T)$. To get finite conductance through the SEP at least three charge states have to be occupied in thermal equilibrium. At $T \ll E_{co}/k_B$ this is only possible near the triple points where three adjacent states are occupied. Here e.g. the sequence $(0,0) \rightarrow (1,0) \rightarrow (0,1) \rightarrow (0,0)$, corresponding to a charge transfer from left to right, occurs with finite probability. The inverse process is equiprobable, but under voltage bias a net current occurs. At $n_x = 1, n_y = -\kappa$

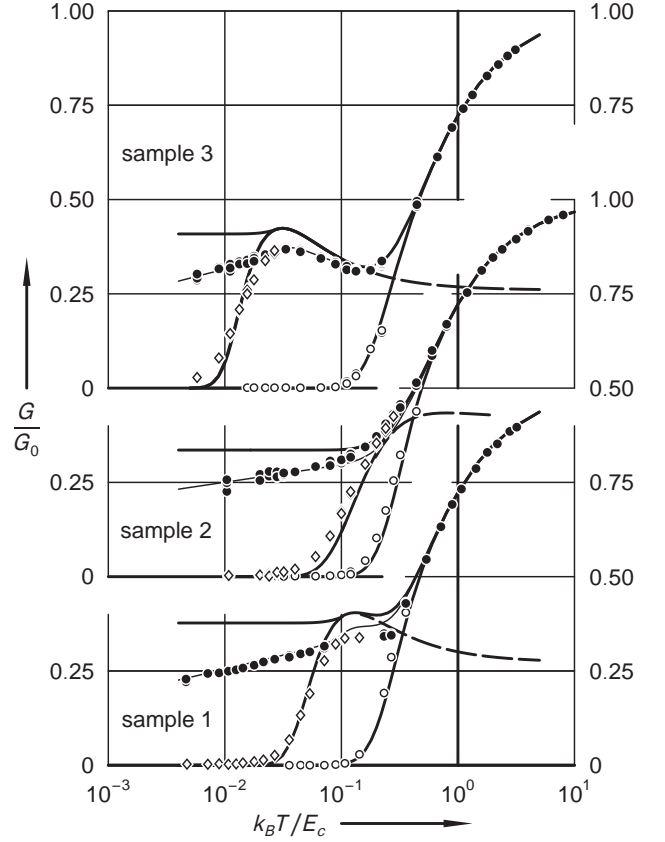


FIG. 4: Linear response conductance of the three samples as a function of temperature. Shown are G_{\min} (\circ), G_{\max} (\bullet), and G_m (\diamond , the conductance at $n_x = 0.5$). The dashed lines are the result of an analytical solution of a 4 state model (see text). As solid lines the outcome of the sequential model with parameters from Tab. I is shown. For the thin solid line a term of the form $\alpha \log(k_B T / E_{co})$ has been added to the maximal conductance as calculated from the sequential model. Here α is a fitting parameter.

where G_m is measured, the charging energy of states $(0,0)$ and $(1,1)$ lie $\Delta E = E_{co}$ above the two fold degenerate ground state $((0,1), (1,0))$. As a result the linear response conductance at $T \ll E_{co}/k_B$, as calculated from the sequential model, is exponentially suppressed since no charge transfer is possible using only two states. At $T \sim E_{co}/k_B$ the states $(0,0)$ and $(1,1)$ are thermally occupied with increasing probability leading first to an exponential increase of G_m and finally to the merging of G_m and G_{\max} . For $n_x = n_y = 0$ states besides $(0,0)$ are occupied for $T \gtrsim E_c/k_B$ only. Thus G_{\min} is exponentially small for $T \ll E_c/k_B$.

The most striking feature of our measurements is the non-monotonic dependence of G_{\max} on the temperature found for sample 3. It is clear from Fig. 4 that the phenomenology is correctly described by the sequential model. To get more insight into the nature of the drop of G_{\max} at $T > E_{co}/k_B$ we analyze $G_m(T)$, which coincides with G_{\max} in the relevant temperature range. The

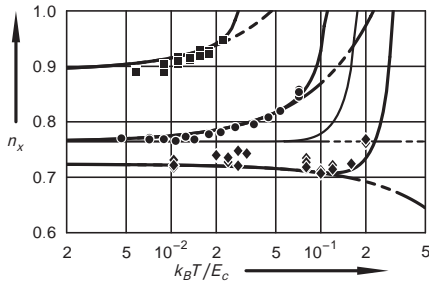


FIG. 5: Position of the conductance maxima as a function of temperature. \bullet : sample 1, \blacklozenge : sample 2, \blacksquare : sample 3. Lines: Predictions of the full sequential model (solid) and Eq. 1 (three-state approximation, dash dotted). For sample 1 the peak position has been used to adjust $g_s/g_m = 5$. Assuming $g_l = g_r = g_m$ gives the thin lines failing to fit the data.

four-state approximation mentioned above yields an analytical solution:

$$G_m^{(4)} = \frac{G_s}{2} \frac{\beta E_{co}}{\sinh(\beta E_{co})} \left(1 - \frac{2g_s}{g_m} \frac{\beta E_{co}}{1 - e^{\beta E_{co}}} \right)^{-1}. \quad (2)$$

We have drawn this function for our sample parameters in Fig. 4 as dashed lines. It has a distinct maximum for $g_m < g_s$, the position and strength of which depends on the ratio g_s/g_m . The above approximation breaks down at $T \sim E_c/k_B$ where more than four states are occupied significantly resulting in a rapid rise of the conductance. For an experimental observation of a local minimum the relation $E_{co} < E_c$ has to be fulfilled in addition to $g_m < g_s$.

In Fig. 5 we plot the n_x coordinate of the conductance maximum n_{\max} as a function of temperature. Again, reasonable agreement with the sequential model is found. For $T \rightarrow 0$ the position of the maximum approaches the location of the triple point. At low temperature the conductance peak is described by Eq. 1. The maximum can shift in either direction depending on the ratio g_s/g_m . This can be used to determine g_s/g_m for sample 1 ($g_s/g_m = 5$) where this ratio can not be measured directly due to the simple layout (see above).

The sequential model fails to predict the temperature dependence of G_{\max} at low temperature. This deviation can be described phenomenologically by adding a term of the form $\Delta G_{\text{qf}} = \alpha \log(k_B T / (2E_{co}))$. The thin solid lines in Fig. 4 display the outcome of a fitting procedure in α that minimizes the mean square deviation between the measured values of G_{\max} and $G_{\text{seq}} + \Delta G_{\text{qf}}(\alpha)$, showing very good agreement. We find $\alpha_1 = 45$ nS, $\alpha_2 = 200$ nS, and $\alpha_3 = 33$ nS for sample 1, 2, and 3, respectively. For the SET much the same behavior is observed and attributed to quantum fluctuations of the charge states. Pohjola et al. [12] analyzed the linear response of the SEP by renormalization group methods. They also found a logarithmic behavior of the low temperature conduc-

tance, in qualitative agreement with our experimental result. However, quantitative results were obtained for certain limiting cases of special interest only. For a detailed comparison with our experiment a calculation using our sample parameters is highly desirable.

In summary we have presented an experimental study of the linear response conductance of the SEP in a regime where quantum fluctuations of the charge eigenstates can not be ignored. Depending on the ratio g_s/g_m the SEP shows a remarkably rich phenomenology even within the framework of lowest-order perturbation theory, the so-called sequential tunneling model. Most strikingly, in the easily accessible regime $E_{co} < E_{cx}$ and $g_m \ll 2g_s$ a pronounced non-monotonic temperature dependence of the conductance has been observed. Phenomena of this kind are to be expected in all single electron devices which are more complex than the SET. They can uncover internal characteristics inaccessible by other means – here e. g. g_s/g_m which is not directly measurable in the most natural SEP layout (sample 1). At low temperature deviations from the sequential behavior due to quantum fluctuations become clearly visible. They are described in close analogy to the SET by a logarithmic correction term of the form $\Delta G_{\text{qf}} = \alpha \log(k_B T / (2E_{co}))$, in qualitative agreement with the findings of Ref. 12. We propose a reevaluation of the formulae of Ref. 12 with parameters in accordance with our experiment so as to check the applicability of perturbation expansion for devices more complex than the SET.

We acknowledge useful discussions with G. Göppert, G. Johansson, P. Joyez, J. König, H. Pothier, and H. v. Löhneysen. This work has been carried out as part of SFB 195.

-
- [1] D. V. Averin and K. K. Likharev, in *Mesoscopic Phenomena in Solids*, edited by B. L. Altshuler, P. A. Lee, and R. A. Webb (Elsevier Science Publishers B. V., Niederlande, 1991), p. 173.
 - [2] G.-L. Ingold and Y. V. Nazarov, in *Single Charge Tunneling*, edited by H. Grabert and M. H. Devoret (Plenum Press, New York, 1992), p. 311.
 - [3] P. Joyez et al., Phys. Rev. Lett. **79**, 1349 (1997).
 - [4] D. Chouvaev et al., Phys. Rev. B **59**, 10599 (1999).
 - [5] C. Wallisser et al., Phys. Rev. B **66**, 125314 (2002).
 - [6] J. König et al., Phys. Rev. Lett. **78**, 4482 (1997).
 - [7] J. König et al., Phys. Rev. B **58**, 7882 (1998).
 - [8] G. Göppert et al., Phys. Rev. B **62**, 9955 (2000).
 - [9] H. Pothier et al., Physica B **169**, 573 (1991).
 - [10] H. Pothier et al., Europhys. Lett. **17**, 249 (1992).
 - [11] S. V. Lotkhov et al., Appl. Phys. Lett. **78**, 946 (2001).
 - [12] T. Pohjola et al., Phys. Rev. B **59**, 7579 (1999).
 - [13] K. P. Hirvi et al., Appl. Phys. Lett. **67**, 2096 (1995).
 - [14] B. Limbach, Tech. Rep. FZKA 6791, Forschungszentrum Karlsruhe (2002), URL <http://bibliothek.fzk.de/zb/berichte/FZKA6791.pdf>.